LIGHTNING FIELD SPECTRA OBTAINED FROM AIRBORNE MEASUREMENTS

B. P. Kuhlman
Air Force Wright Aeronautical Laboratories, Dayton, Ohio
J. S. Reazer
Technology/Scientific Services, Incorporated, Dayton, Ohio
W. P. Geren
Boeing Military Airplane Company, Seattle, Washington
P. L. Rustan
Air Force Institute of Technology, Dayton, Ohio

ABSTRACT

A WC-130 aircraft was used as an airborne platform for broadband electric and magnetic field sensors to measure the surface fields on the airframe from lightning strikes in the 7 - 35 km range. The waveforms were recorded digitally, with a sample interval of 20 nsec and a time window of 164 microseconds. Since the aircraft was above 15,000 feet, and the lightning source was relatively nearby, the effects of ground propagation were minimized. Spectra have been obtained for the stepped leader, first return stroke, and subsequent return stroke over the frequency range 100 kHz to 20 MHz. These spectra are compared to published data of lightning field spectra obtained from ground-based measurements. With airframe resonances and field enhancement effects removed, the data have two primary applications:

(1) To add to the data base for the nearby lightning strike threat; and

(2) To infer characteristics of the stepped leader, first return stroke, and subsequent return stroke processes.

Recommendations for these applications are presented.

ATTENTION HAS BEEN GIVEN in recent years to characterization of unwanted sources of electromagnetic interference, such as lightning or nuclear EMP, that may interact with aircraft and impair mission capability. The use of non-metallic airframe materials and solid-state avionics aggravates the problem by reducing electromagnetic shielding and lowering damage or upset thresholds on new generation aircraft. Measurements of lightning fields and currents, indicating the level of the hazards, have been made on the ground for several years. Recently, wide bandwidth measurements of lightning fields and currents have been recorded on aircraft in flight to obtain a more pertinent threat characterization. As a part of this characterization, it is necessary to consider the electromagnetic effect of the aircraft on the measurements so that a generic threat definition may be derived.

In 1979 the Air Force Flight Dynamics Laboratory, in conjunction with the National Oceanic and Atmospheric Administration (NOAA), initiated a three-year program to measure the properties of lightning encountered in flight (1). A NOAA WC-130 "Hurricane Hunter" aircraft was fitted with sensors for measuring nearby and direct lightning strikes. A sophisticated data acquisition system designed for repetitive wide bandwidth transient measurements was developed by the Micro Pro Company and installed in the WC-130. More than one hundred flight hours were logged over the three-year period and several hundred wide bandwidth lightning measurements were recorded. Progress and results of this research are documented in references (1) through (4).

In this paper, we have analyzed the frequency characteristics of three lightning transients -- stepped leader pulses, first return strokes, and subsequent return strokes, recorded on the WC-130. Wide bandwidth magnetic field measurements were Fourier transformed, averaged, and normalized for range. The results are compared with published frequency spectra from similar field measurements obtained on the ground.

INSTRUMENTATION

The sensors and instrumentation used on the WC-130 have been described in detail in reference (4). The specific equipment used to obtain the data for this study are reviewed next. Magnetic field waveforms were obtained from a single wideband sensor mounted on the centerline of the upper fuselage of the WC-130 approximately seven meters from the nose of the aircraft ($\dot{B}_1$ in Figure 1). The sensor was an EG&G model CML-7 cylindrical Moebius loop B-Dot sensor (5,6) that produces an output voltage proportional to the derivative of the magnetic field over a 38 MHz bandwidth. A second B-Dot sensor ($\dot{B}_2$) was positioned adjacent to the first and oriented to respond to magnetic flux parallel to the wing axis as shown in Figure 1. This sensor was used in conjunction with $\dot{B}_1$ and an electric field sensor to assist in locating the lightning strikes. The arrows in Figure 1 indicate the direction of increasing field for a positive sensor output voltage.

B-Dot sensor outputs were transmitted through Merit fiber optic data links to instrumentation inside the aircraft. The signals were logarithmically compressed, digitized, and encoded on magnetic tape. A partial block diagram of the instrumentation is shown in Figure 2. The digitizing was performed with a Micro Pro model PR7901 digital transient recorder with a 20 ns sample period, 8 bit amplitude resolution and 164 μs sample window. Forty microseconds of pretrigger sampling was programmed into the digitizer so that leader pulses preceeding return strokes could be recorded.

An electric field sensor was mounted directly ahead of the B-Dot sensors on the upper fuselage of the aircraft. The sensor output was integrated electronically and recorded on two wideband FM channels of a Honeywell model 101 analog tape recorder. Recorded bandwidth of the electric field was 0.1 Hz to 500 kHz. The analog recorder also recorded a logic pulse indicating the time of digital transient recorder triggering. Trigger pulse location within the overall electric field waveform was the first criteria used to categorize the digitized data (Figure 3). Refinement of the categorization was obtained through examination of the fine structure of the digitized waveform.

AIRCRAFT EFFECTS - We have simplified the interpretation of the magnetic field measurements to a certain degree by careful positioning of the B-Dot sensor. By positioning the sensor in the plane defined by the wings and upper fuselage surface, and orienting it to respond to magnetic flux parallel to the fuselage axis and perpendicular to the wing structure, we have made it in-

sensitive to magnetic fields and resonances associated with axial wing and fuselage current flow. Some coupling of resonant responses is evidenced in the time domain waveforms due to non-ideal symmetry (8).

Field enhancement due to the aircraft structure can be determined in the manner described by Taylor (9,10). The aircraft fuselage is modeled as a cylinder with the axial component of the magnetic field at the surface given by

$$H_l \simeq H_l{}^{inc}\ (1-j2ka\cos\theta)$$

where $H_l{}^{inc}$ is the incident magnetic field, a is the fuselage radius, $k=2\pi/\lambda$ and θ is measured upward from the direction of incidence along the fuselage circumference. This equation is valid for broadside incidence where $(ka)^2<<1$. For most of our data, the aircraft is positioned so that the cosine function in the second term goes to zero. In the worst case, θ would be 45^o and the second term would result in an enhancement of high frequencies. This enhancement would be below 3 dB at 20 MHz, however, and less at lower frequencies. Therefore, the resultant magnetic field parallel to the fuselage axis at the $\dot{B}_l$ sensor location is approximately equal to the incident magnetic field at this point.

RANGE DETERMINATION - Distances to thunderstorms were determined from radar patterns obtained during flight. The radar data were recorded on digital tape and processed later by computer for analysis. Lightning data were selected from storm cells that could be clearly identified. When several storm cells were active around the aircraft, ambiguities in locations were resolved by examining the polarities and relative amplitudes of the B-Dot signals. Since the precise location of the return stroke within storm cells was unknown, lightning location accurscy deteriorated with decreasing thunderstorm range.

DATA PROCESSING

The digitized lightning data was scaled, anti-logged and numerically integrated to display the field waveshape. A typical overall data window and the integration are shown in Figure 3. A 10.24 μs (512 sample points) time interval containing the data of interest was selected from the overall waveform for processing. For first return strokes, the interval was chosen to include the slow front of the field waveform but to exclude stepped leader pulses. Consequently, the derivative impulse corresponding to the fast front of the return stroke was placed about 2 to 4 μs after the beginning of the interval. Figure 5 shows a first return stroke derivative waveform and the numerical integration recorded at 9 kilometers. Subsequent return stroke waveforms were positioned approximately 1 to 2 μs after the beginning of the 10.24 μs interval. For stepped leader pulses, 4 μs of data containing the pulse was positioned at the beginning of the interval and the remaining 6.24 μs set to zero. Subsequent stroke and stepped leader waveforms are shown in Figures 6 and 7, respectively.

A fast Fourier transform of the data was calculated using a rectangular window according to the following equation:

$$X(mF) = T\sum_{n=0}^{N-1} x(nT)e^{-j(2\pi mn/N)}$$

where T is the sample interval, N is the number of samples, $F = 1/NT$, $m = 0,1,\ldots, N/2$, $x(nT)$ is the sampled magnetic field data, and $X(mF)$ is the complex spectra value (7). With 512 samples and a 20 ns sample period, spectra values are calculated at discrete frequency increments of approximately 97 kHz. Since field derivatives were recorded, the time waveform was near zero at the beginning and end of the 10.24 μs interval, minimizing errors introduced by abrupt transitions at the boundaries of the window. Magnitudes of the frequency spectra were normalized to a distance of 50 km assuming a 1/r relationship, where r is the distance from the thunderstorm to the aircraft, and corrected for angle of incidence to the sensor by dividing by the sine of the angle from the aircraft nose to thunderstorm location. Spectra magnitudes were then averaged at each frequency and standard deviations calculated. The derivative response of the sensor was accounted for by dividing the spectra magnitudes by radian frequency ω. The resulting values were expressed in decibels using

$$\overline{H}\ (\omega)(dB) = 20\ Log_{10}\left[\overline{|H(j\omega)|}\right]$$

where the horizontal bar $\overline{\quad}$ denotes mean and the vertical bars $|\ |$ denote magnitude. Standard deviations ($\sigma(\omega)$) were referenced to average values and expressed in decibels using

$$SD\ (\omega)(dB) = 20\ Log_{10}\left[\overline{|H(j\omega)|} + \sigma(\omega)/\overline{|H(j\omega)|}\right]$$

RESULTS

The data were recorded during several storms occurring on 25 August and 26 August 1981 at an altitude of 5.2 km. Ten first return strokes at a range of 11 km to 35 km and nine subsequent return strokes at a range of 7 km to 28 km were selected for processing. The last stepped leader pulse preceeding the return stroke was processed from nine of the first stroke waveforms. Subsequent strokes showing dart-stepped leaders were excluded from the data set.

Average spectra values for first return strokes, subsequent strokes and leader pulses are plotted in Figures 8 through 10, respectively. A linear interpolation between data points is also plotted. Spectra magnitudes at selected frequencies are tabulated in Table 1 along with standard deviations.

TRENDS IN SPECTRA WITH FREQUENCY - Average spectra values at 100 kHz are -142 dB for both first and subsequent return strokes and 20 dB lower for leader pulses. All three sets of data

decrease approximately inversely with frequency (f) to about 1 MHz and decrease more rapidly at higher frequencies. Approximate trends in average spectra amplitude with frequency are summarized in Table 2.

First stroke spectra show a decrease proportional to $1/f^2$ from 800 kHz to 5 MHz. Beyond 5 MHz there is a slight dip in the spectra and then the amplitudes tend toward 1/f dependence.

Subsequent stroke spectra maintain the initial 1/f slope from 100 kHz out to 1.2 MHz and then decrease rapidly until 3.5 MHz. This spectra also regains a 1/f slope by 20 MHz.

Leader pulses show less relative energy at low frequencies with a decrease of 16 dB from 100 kHz to 1 MHz rather than 20 dB as in the case of the return strokes. Beyond 1 MHz the spectra decreases proportional to 1/f.

Evidence of aircraft resonances is visible in the graphs in the 3 to 5 MHz region.

STANDARD DEVIATIONS - Standard deviations are greatest for leader pulse spectra and smallest for subsequent stroke spectra as indicated in Table 1. The larger leader pulse standard deviations are indicative of the more random structure of the leader waveshapes as well as a lower signal to noise ratio. Since leader pulse data were extracted from the return stroke waveforms, the signal to noise ratio would be a factor of two to five lower for leader pulses than for first return strokes (for derivative magnetic field data). Subsequent stroke standard deviations are low, particularly at lower frequencies, suggesting uniformity in different return stroke waveshapes.

COMPARISON TO PUBLISHED SPECTRA - Frequency spectra derived from broadband ground-based electric field measurements have been obtained by Serhan (11) and more recently by Weidman (12). Serhan calculated spectra from 2 kHz to 700 kHz for measurements recorded from 1.5 km to 200 km. Weidman obtained spectra of electric fields from 100 kHz to 20 MHz for measurements at 30 to 50 km where propagation was over saltwater so that the effects of ground wave attenuation were minimized.

Weidman's data for first return strokes show a spectral amplitude of about -95 dB at 100 kHz, a slope of 1/f to 2 MHz, $1/f^2$ to 10 MHz, and $1/f^5$ beyond 10 MHz. These trends are similar to the WC-130 data with two exceptions -- the transition from slopes of 1/f to $1/f^2$ occurs at 800 kHz rather than 2 MHz; and the data shows no rapid decrease in spectral amplitude beyond 10 MHz for the aircraft data.

A comparison in spectral amplitudes between the air and ground-based data is difficult for several reasons. For identical waveshapes, spectra amplitudes should be proportional to waveform amplitudes. With different frequency characteristics, however, the proportionality becomes a function of frequency. Also, aircraft waveforms are obtained at varying range and elevation from the return stroke which precludes a direct comparison with ground-based data at a fixed position. Examination of the first stroke data shows a ratio of 112 to 1120 for electric field spectra on the ground versus magnetic field on the aircraft over a 500 kHz to 5 MHz frequency range. This bounds the impedance of free space (377Ω) that would be expected for simultaneous, distant, ground-based electric and magnetic field data (13).

SUMMARY

We have calculated the frequency spectra of broadband lightning magnetic field measurements recorded on a WC-130 aircraft in flight. The data were recorded at a range of 7 to 35 km. Spectra values were calculated from 100 kHz to 20 MHz for stepped leader pulses, first return strokes and subsequent return strokes. Spectra amplitude trends with frequency were extracted and compared with trends of published ground based spectra. From the data we can infer the following lightning characteristics:

1. First and subsequent return strokes have similar energy levels in the 100 kHz to 20 MHz frequency range.
2. The initial transition point from slopes of 1/f to steeper slopes, occurring at 800 kHz for first strokes and 1.2 MHz for subsequent strokes, is probably indicative of faster subsequent stroke risetimes.
3. Leader spectra lie 14 to 20 dB below first stroke spectra at low frequencies suggesting a factor of 5 to 10 difference in magnetic field amplitude.
4. Subsequent stroke spectra show a relatively small standard deviation suggesting a uniformity of waveshape among independent return strokes. Although some of these characteristics could be observed from time domain waveforms, one significant feature that is extracted by Fourier analysis is the presence of high frequency energy beyond 10 MHz that is not observed with ground-based measurements. From our analysis, this does not appear to be characteristic of the recording system or airframe enhancement but rather an inherent feature of the lightning fields.

REFERENCES

1. R.K. Baum, "Airborne Lightning Characterization." Proceedings of the NASA Symposium on Lightning Technology, NASA CP2128, April 1980.
2. R.K. Baum et al., "Airborne Electromagnetic Characterization of Lightning." Proceedings of the International Aerospace Conference on Lightning and Static Electricity, Oxford, England 1980.
3. P.L Rustan, et al., "Correlated Airborne and Ground Measurement of Lightning." Proceedings of the International Aerospace Conference on Lightning and Static Electricity, Oxford, England 1982.
4. P.L. Rustan, et al., "Airborne Lightning Characterization," USAF Technical Report, AFWAL-TR-83-3013, April 1983.
5. C.E. Baum, et al., "Sensors for Electromagnetic Pulse Measurements Both Inside and Away from Nuclear Source Regions." IEEE Transactions

on Antennas and Propagation, Vol AP-26, No. 1, January 1978.

6. "CML Sensors (Full Loop), "EG&G Washington Analytical Services Center, Data Sheet 1106, September 1980.

7. "TEK SPS Basic Signal Processing Package." V01 CP91171, SPS Information Group, February 1977.

8. C.E. Baum, "Interaction of Electromagnetic Fields with an Object Which has an Electromagnetic Symmetry Plane." Air Force Weapons Laboratory EMP Interaction Notes, No. 63, March 1971.

9. C.D. Taylor, "External Interaction of the Nuclear EMP with Aircraft and Missles." IEEE Transactions on Electromagnetic Compatibility, Vol EMC-20, No. 1, February 1978.

10. W.P. Geren, "Calibration of C-130 Lightning Characterization Sensors." Air Force Contract F33615-81-C-3409 Final Report, AFWAL-TR-82-3095, December 1982.

11. G.I. Serhan, et al., "The RF Spectra of First and Subsequent Lightning Return Strokes in the 1- to 200- km Range." Radio Science, Vol 15, No. 6, December 1980.

12. C.D. Weidman, E.P. Krider, M.A. Uman, "Lightning Amplitude Spectra in the Interval from 100 kHz to 20 MHz." Geophysical Research Letters, Vol 8, No. 8, August 1981.

13. M.A. Uman, et al., "Correlated Electric and Magnetic Fields From Lightning Return Strokes." Journal of Geophysical Research, Vol 80, January 1976.

Table 1 - Average Spectra Values and Standard Deviations in Decibels

Frequency	First Strokes		Subsequent Strokes		Leaders	
	Mean	SD	Mean	SD	Mean	SD
100 kHz	-142	2.4	-142	2.1	-162	4.2
200 kHz	-152	4.5	-146	2.2	-166	3.5
500 kHz	-158	3.7	-156	2.8	-172	3.1
1MHz	-170	3.1	-164	2.5	-179	4.0
2MHz	-177	3.4	-177	3.0	-191	4.3
5 MHz	-196	4.2	-196	4.0	-205	4.2
10 MHz	-210	3.5	-209	3.3	-216	3.9
15 MHz	-213	2.9	-215	5.2	-220	3.6
20 MHz	-218	4.6	-221	4.6	-225	4.7

Table 2 - Variations of Spectra Amplitude with Frequency

First Return Strokes		Subsequent Return Strokes		Leader Pulses	
Frequency Range	Trend	Frequency Range	Trend	Frequency Range	Trend
0.1 - 0.8 MHz	1/f	0.1 - 1.2 MHz	1/f	0.1-1.0MHz	-16dB/decade
0.8 - 5.0 MHz	$1/f^2$	1.2 - 3.5 MHz	$1/f^3$	1.0 - 20 MHz	1/f
5.0 - 20 MHz	1/f	10 - 20 MHz	1/f		

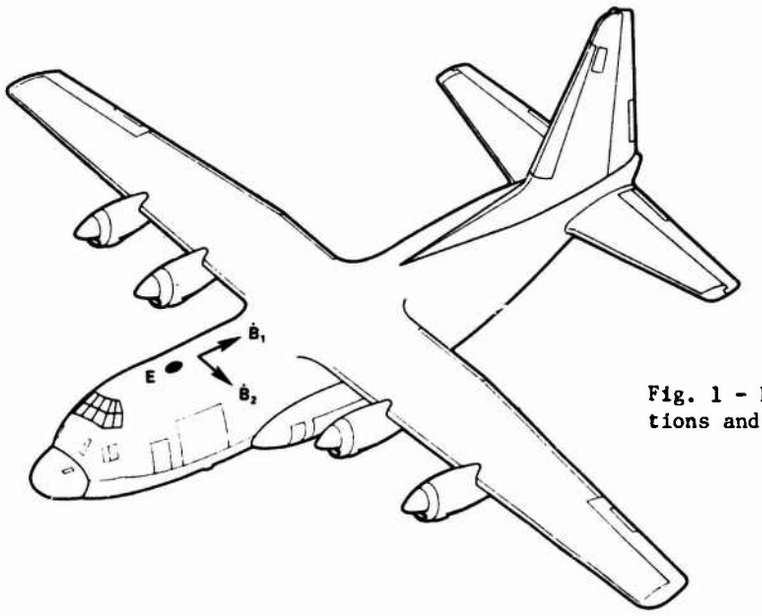

Fig. 1 - NOAA WC-130 aircraft with sensor locations and magnetic field orientations

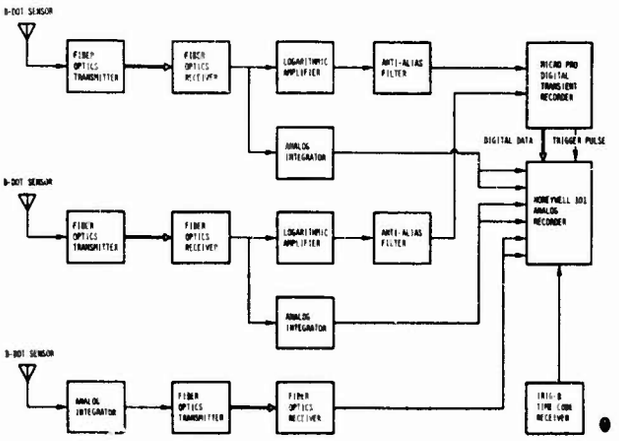

Fig. 2 - Block diagram of aircraft instrumentation

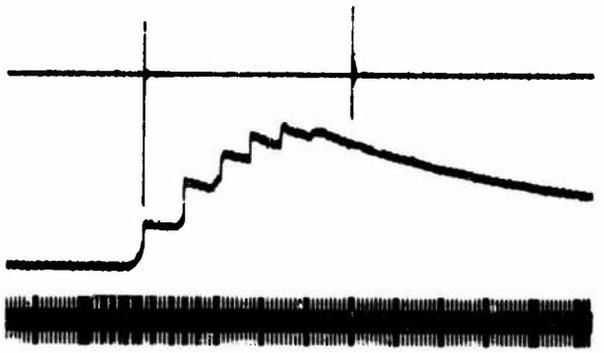

Fig. 3 - Strip chart of aircraft electric field (center trace), digital trigger pulse (first pulse on top trace) and IRIG-B time code (bottom trace)

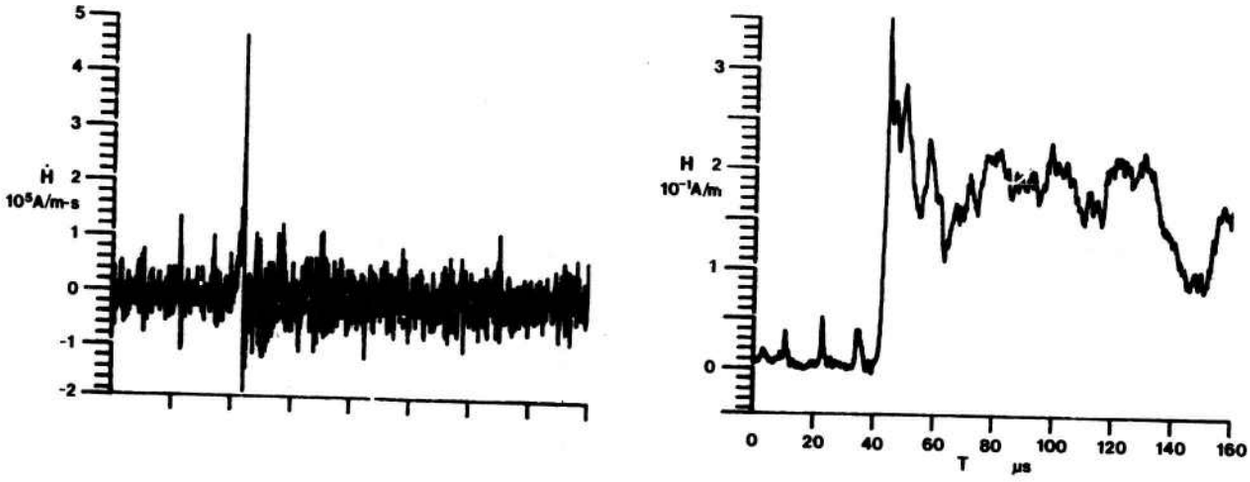

Fig. 4 - Overall graph of digital magnetic field derivative data ($\dot{H}$, top trace) and the numerical integration (bottom trace)

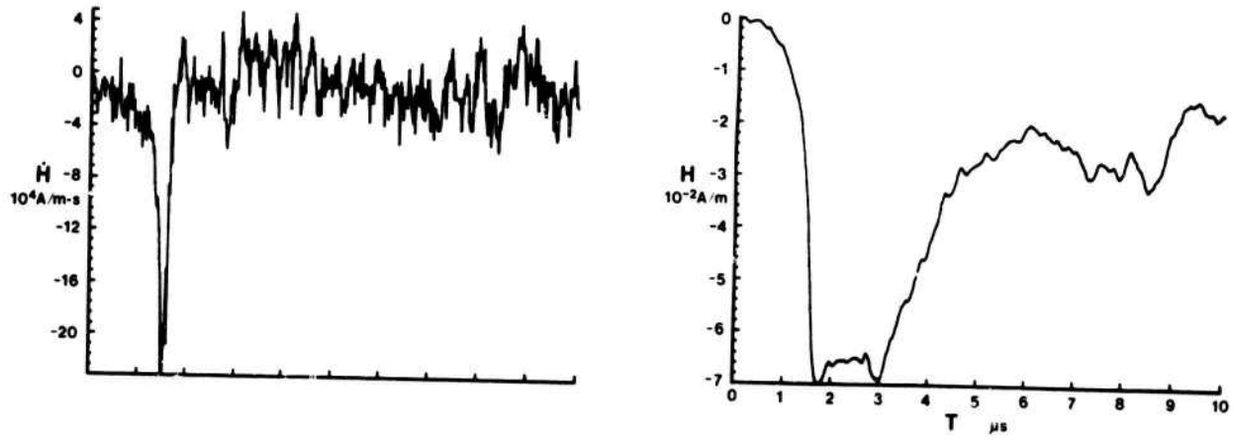

Fig. 5 - Ten microsecond data window for first return stroke waveform at 9.5 km with numerical integration

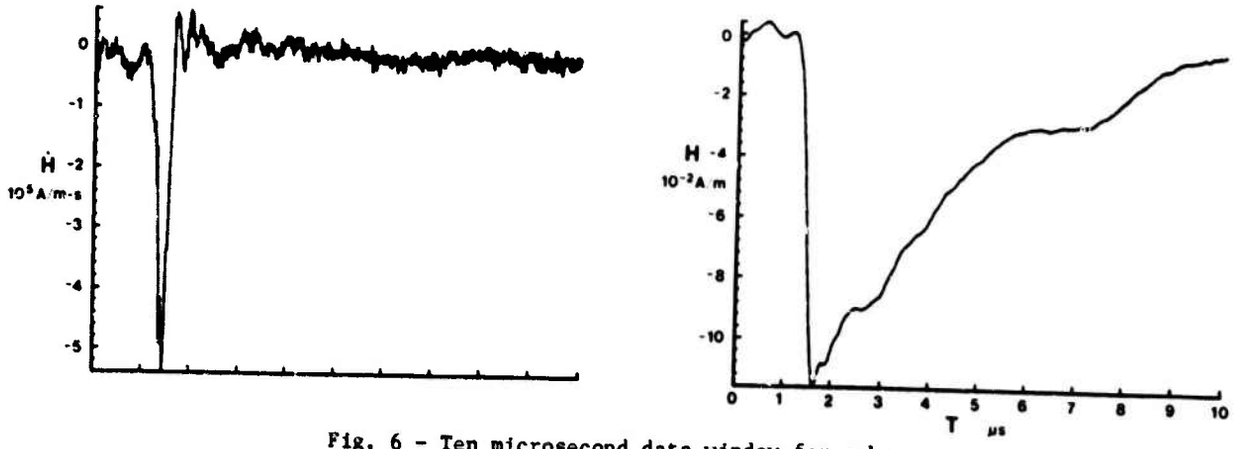

Fig. 6 - Ten microsecond data window for subsequent return stroke waveform at 10.4 km with numerical integration

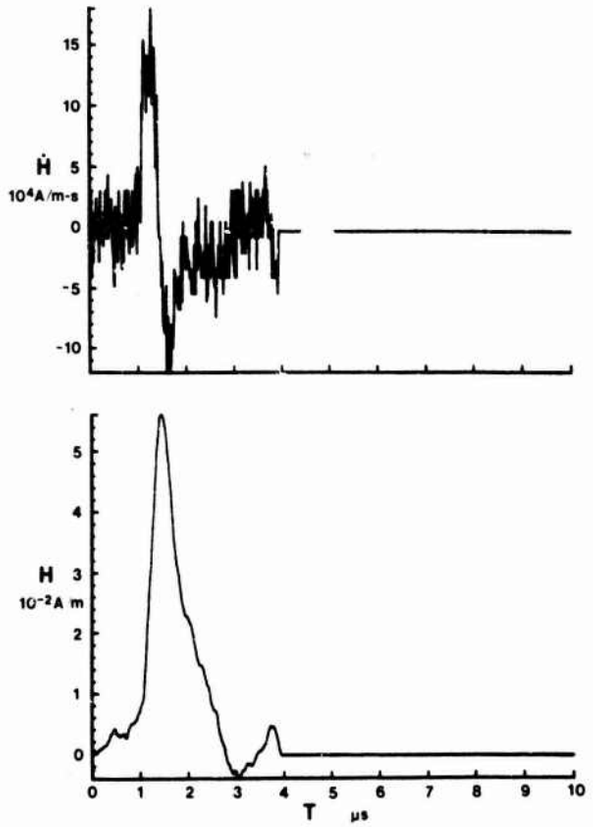

Fig. 7 - Ten microsecond data window for leader pulse waveform at approximately 11 km with numerical integration

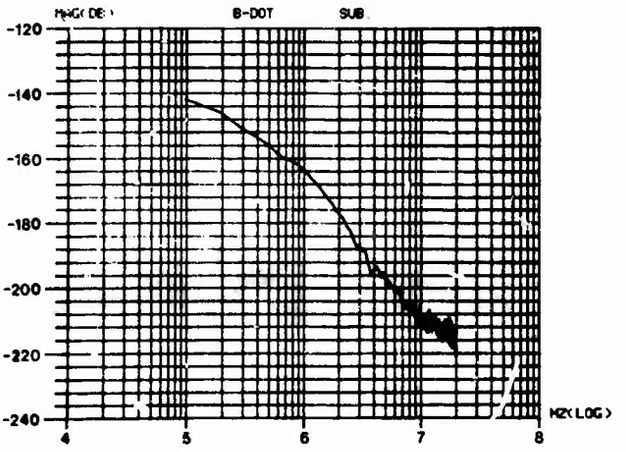

Fig. 9 - Graph showing average spectra amplitude in dicibels versus log frequency for subsequent return strokes

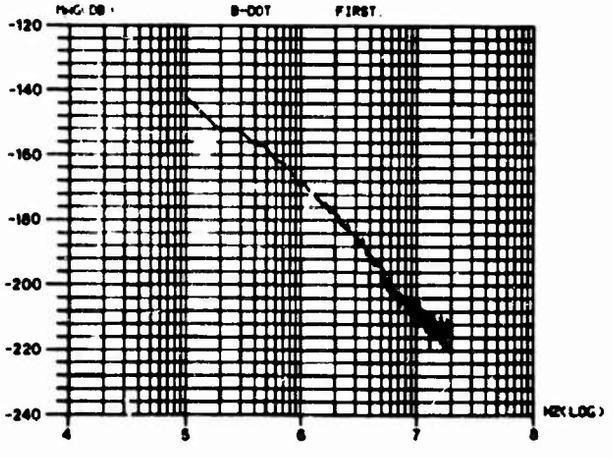

Fig. 8 - Graph showing average spectra amplitude in decibels versus log frequency for first return strokes

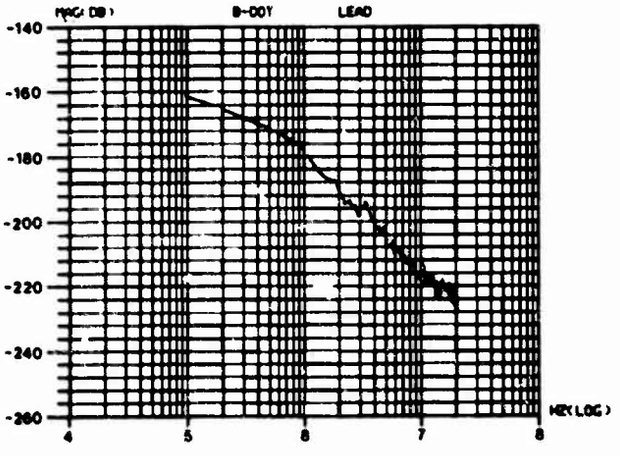

Fig. 10 - Graph showing average spectra amplitude in decibels versus log frequency for leader pulses